Available online at www.sciencedirect.com
SCIENCE DIRECT®
International Journal of Multiphase Flow 30 (2004) 853–876
International Journal of Multiphase Flow
www.elsevier.com/locate/ijmulflow

Characteristics of developing free falling films at intermediate Reynolds and high Kapitza numbers ☆

E.I.P. Drosos, S.V. Paras, A.J. Karabelas *

Chemical Process Engineering Research Institute, and Department of Chemical Engineering, Aristotle University of Thessaloniki, Univ. Box 455, GR 54 124 Thessaloniki, Greece

Received 7 December 2003; received in revised form 10 March 2004

Abstract

Experiments on developing free falling films have been carried out in a vertical rectangular channel, using smooth inlet conditions, with three liquids characterized by high Kapitza numbers, *Ka* (i.e. water, 1.5% butanol and 2.5% butanol solutions with surface tension 75, 50 and 40 mN/m, respectively) at intermediate Reynolds numbers ($Re_L < 400$). Film thickness measurements supported by visual observations suggest that reduced surface tension significantly affects the inception of waves at the entrance region of the film. However, no significant qualitative difference is observed concerning developing wave patterns in the longitudinal direction, as large ''tear-drop'' type waves appear downstream in all cases, with the smaller *Ka* liquids being more unstable as expected. The new data show that above $Re_L \sim 200$, the RMS values of film thickness fluctuations, beyond the wave inception region, tend to be nearly independent of Re_L. Results concerning other typical falling film characteristics also show that above $Re_L \sim 200$ (for the Re_L range of the present experiments) the wave structure is weakly dependent on Re_L beyond the wave inception region. The dominant disturbance frequencies on the wavy film surface as well as the wave celerity are in good agreement with earlier findings. Finally, results from previous linear stability analyses are compared with the new data showing in general satisfactory agreement especially with measurements corresponding to developing nearly two-dimensional waves.

Keywords: Free falling film; Vertical plate; Intermediate Reynolds number; High Kapitza numbers

☆ It is our great pleasure to contribute to this Festschrift honoring Professor George Yadigaroglu, our esteemed colleague and friend. We congratulate him, on the occasion of his 65th birthday, for his scientific contributions and other achievements, and wish him all the best!

* Corresponding author. Tel.: +30-2310-996201; fax: +30-2310-996209.
E-mail address: karabaj@cperi.certh.gr (A.J. Karabelas).

0301-9322/$ - see front matter © 2004 Elsevier Ltd. All rights reserved.
doi:10.1016/j.ijmultiphaseflow.2004.03.003

1. Introduction

Well known is the significant role played by falling films in a wide variety of naturally occurring phenomena, as well as in the operation of industrial process equipment where heat and mass transfer take place. The quest for more efficient and compact equipment, such as reactors and condensers usually made of vertical compartments (e.g. Paras et al., 2001), is partly responsible for the sustained interest in improving our understanding of falling film characteristics. The typical height of this type of compact equipment is of order 1 m. Controlled laboratory experiments (e.g. Alekseenko et al., 1994) show that, over such a length, falling films tend to evolve from an initially uniform liquid layer with smooth surface to a complex state in which two-dimensional waves appear first, developing downstream into three-dimensional (rather large) waves or "humps", moving on a thin substrate. The scope of this work is to better understand the characteristics of such *developing* falling films under conditions relevant to practical applications, i.e. at intermediate *Reynolds numbers*, Re_L, $(60 < Re_L < 360)$ and high *Kapitza numbers*, *Ka*, $(1650 < Ka < 3500)$. In this work Re_L and *Ka* are defined as

$$Re_L = \frac{4\Gamma}{\mu} \tag{1}$$

$$Ka = \frac{\sigma}{\rho g^{1/3} \nu^{4/3}} \tag{2}$$

where Γ is the liquid mass flow rate per unit width of the plate, σ is the surface tension, μ and ν the dynamic and kinematic viscosity, respectively. The particular problem motivating the present study is the counter-current gas/liquid flow through vertical channels, where the role played by the gravity-induced wavy film is dominant. Understanding the latter is considered a first step before introducing the complication of counter-current gas convection.

A great deal of work has been published on free falling films, concerning mainly flow development *inside* or *outside a tube at moderate to high Reynolds numbers* (Re_L). The following brief literature survey is concerned mostly with developing film flow. Tailby and Portalski (1962), Portalski (1963) and Portalski and Clegg (1972) studied experimentally the inception region and the initial wave formation for water and several other liquids at moderate to high Re_L. Statistical film characteristics at long distance from liquid entry were obtained by Chu and Dukler (1974) at moderate to high Re_L where pseudo-laminar and turbulent flow is expected to occur. Salazar and Marschall (1978) measured the local thickness by using a light scattering technique. Their results indicated clearly the importance of measurement location on film characteristics. Takahama and Kato (1980) studied the flow characteristics of longitudinally developing liquid films, including laminar/turbulent transition along the outer wall of a fairly long vertical tube at high Re_L. An experimental investigation of excited periodic two-dimensional waves was carried out by Alekseenko et al. (1985, 1994) with water/glycerin and water/alcohol solutions as working fluids at low to moderate Re_L. They showed that solitary waves are traveling in stationary patterns with almost constant celerity and examined the evolution of excited disturbances of various forms as well. Nakoryakov et al. (1987) continued these experiments in order to examine the influence of waves on interfacial mass transfer, but they also studied the flow patterns of free falling films at low to high Re_L. Karapantsios et al. (1989) and Karapantsios and Karabelas (1995) carried out

experiments inside a vertical pipe at moderate to high Re_L, investigating also the longitudinal characteristics of falling films far away from the liquid entry point. An image-processing system developed by Patnaik and Perez-Blanco (1996) facilitated the identification of single frequency roll waves in developing films. The study of Adomeit and Renz (2000) focused on the hydrodynamics of naturally excited waves inside a vertical tube at moderate to high Re_L and confirmed the three-dimensional character of the wave structure, which is strongly affected by wave interactions. Finally, a study by Ambrosini et al. (2002) deals with the statistical characteristics of the water film surface at various temperatures.

There is a rich literature on theoretical treatments of falling film hydrodynamics where two-dimensional waves are considered. Aside from the pioneering study of Kapitza (1964) on film flow instability, Benjamin (1957) and Yih (1963) concentrated on the analytical treatment of the Orr–Sommerfeld (OS) equation and showed that film flow with a smooth surface is always unstable. Their study, however, was limited to flows with small Re_L and small wave numbers. Similar results were obtained numerically by Anshus and Goren (1966), Krantz and Goren (1971), Anshus (1972) and Pierson and Whitaker (1977), who extended the linear stability analysis to higher Re_L. These studies involve mainly linear stability theory, which predicts the critical conditions and the corresponding characteristics of small amplitude sinusoidal waves near the inception line. Thus it is inadequate for describing fully developed waves at fairly large distances from the inlet, where a chaotic three-dimensional wave motion is observed and improved treatments are required. Benney (1966) was the first to derive an asymptotic expansion procedure for wave disturbances of finite amplitude that is accurate when the wavelength is large compared with the film thickness. This model known in the literature as the long-wave equation (LW), is widely used predicting critical conditions for wave inception and the characteristics of small amplitude two-dimensional waves for low Re_L. A weakly non-linear expansion for large surface tension fluids and for amplitudes of the same order as wave length was first carried out by Lin (1974) and led to the Kuramoto–Sivashinsky (KS) equation that is frequently used due to its simplicity. Alekseenko et al. (1985) proposed a model to describe non-linear non-stationary waves in a wide range of Re_L. Khesghi and Scriven (1987) studied numerically the evolution of finite-amplitude two-dimensional disturbances to a steady flow down a vertical plate, investigating the dependence of wave growth on physical properties and plate length. A theoretical analysis of non-linear two-dimensional waves was also made by Trifonov and Tsvelodub (1991), who studied the dependence of wave characteristics on Re_L and Weber number (We). Hydrodynamics of wave formation on free falling films has been reviewed by Chang (1994); his work (Chang, 1989; Chang et al., 1993) is focused mainly on the LW and KS equations and the results are limited to very small Re_L and high Kapitza (Ka) numbers for which the amplitude is rather small (about 10% of the mean film thickness). Chang has also derived analytical expressions relating film thickness and wave velocity with liquid properties (Chang, 1989). A model describing the dynamics of large amplitude non-periodic waves (with peak to substrate ratios of 3–4) on laminar falling wavy films at high Re_L was presented by Yu et al. (1995). Nguyen and Balakotaiah (2000) continued this study developing a new simplified model for describing wave evolution at low Re_L and a broad range of Ka. It is worth mentioning that further efforts to enrich the structure of the wave evolution process by adding a third dimension (leading to a more complex equation) did not result in a significant improvement over simpler models such as the KS equation (Chang, 1994; Nguyen and Balakotaiah, 2000).

The above brief review suggests that, despite progress made in recent years, significant gaps exist in understanding and modeling the evolution of falling films. To contribute in this direction, the present work aims at obtaining complete sets of detailed data on developing film flow down a *vertical plate* for *intermediate* Re_L, at various locations along the plate, including the region near wave inception. Particular attention was paid to vary the Kapitza number (by varying surface tension) without modifying the liquid viscosity. Data with such fluids are lacking.

A description of the experimental equipment and procedures is presented first. Visual observations are reported next on the evolution of waves on falling films providing a qualitative description of flow patterns. Detailed film thickness data and their statistical analysis (for various flow conditions and liquids employed) are reported and discussed next. Finally comparisons are made of the new data with published theoretical and experimental results.

2. Experimental setup and procedures

An experimental facility was specifically constructed to study developing falling film characteristics as well as counter-current gas/liquid flow (Fig. 1). Experiments were carried out in a 70 cm high by 12 cm wide vertical rectangular channel made of Plexiglas® in order to facilitate visual observations. The spacing between the two parallel plates is 10 mm and the length of the plate on which the film flow develops is 38 cm. The liquid phase is introduced uniformly near the top of the channel through a *porous section*, made of stainless steel, with nominal pore size 100 μm (covering the entire active channel width) and embedded flush with the main flat surface in order to facilitate smooth liquid entry. Care was taken to uniformly feed the liquid and to minimize external disturbances upon film formation, by fixing a small liquid reservoir right behind the porous segment, which formed one of the reservoir walls. The liquid drained from the bottom of the channel and was collected in a 50 l storage tank for re-circulation. The liquid flow rate was measured by a bank of calibrated rotameters covering the range of the present experiments ($\sim$0.1 to $\sim$0.7 l/min). Flow adjustment was achieved by a combination of valves and a by-pass. Experiments were conducted at ambient temperature and pressure conditions. Due to the sensitivity of the longitudinal flow development to geometrical imperfections, the channel was carefully aligned in the vertical direction. It should be added that before each set of experiments the inner surface of the Plexiglas® test section was cleaned by a dilute detergent solution and additionally its wetability was improved by treating it with a silica sol solution.

Three liquids were used, i.e. *water*, 1.5% and 2.5% w/w *aqueous butanol solutions*, with physical properties listed in Table 1. Tap water was used for experiments as well as for preparing the butanol solutions after cartridge filtration. Dilute solutions of butanol were employed to obtain significantly smaller surface tension, with practically no effect on the density and viscosity, compared to water. The stability of the butanol solutions was checked prior to and after each experiment by measuring the surface tension and was found to be satisfactory (with an uncertainty of about 5%).

The film thickness measurements reported in this work were taken along the middle of the plate, with probes located at 5 different distances from the liquid entry; i.e. 8, 19, 22, 33 and 36 cm, using the well-known "parallel-wire conductance technique" described elsewhere (e.g. Paras and Karabelas, 1991). This technique relies on the fact that the conductance between two parallel

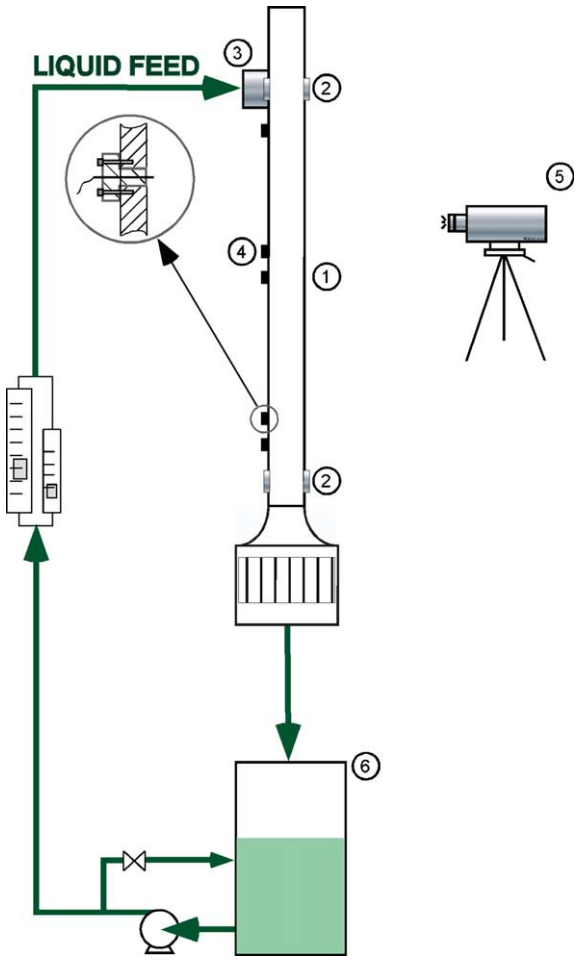

Fig. 1. Schematic diagram of experimental flow loop: (1) cross-sectional view of the test section; (2) porous sections; (3) small reservoir for liquid feeding; (4) measurement stations-probes; (5) camera position; (6) liquid storage tank.

Table 1
Physical properties of the liquids used

	Water (W)	1.5% Butanol (B1)	2.5% Butanol (B2)
ρ, kg m^{-3}	1000	995	980
μ, mPa s	1	1.03	1.09
σ, mN m^{-1}	75	50	40
$Ka(=\sigma/\rho g^{1/3}\nu^{4/3})$	3500	2240	1650

wires is uniquely related to the liquid level between them. Each conductance probe consists of a pair of short parallel *chromel* wires spaced ~2 mm apart with a diameter of 0.5 mm and a length of 2.5 mm. These short and rigid chromel wires are fixed in a removable plug made of Plexiglas® in order to be withdrawn and calibrated outside the test section. It must be noted that the

relatively large wire diameter (0.5 mm) is generally undesirable, since thick wires inside the flow tend to disturb the free falling film. However, the wires are chosen to be rigid enough to allow ex situ calibration and to remain unaffected by the high gas flow-rates that will be used in counter-current flow in future work. To compensate for temperature effects on liquid conductivity, the latter was measured prior to and after each set of experiments and a correction factor was incorporated in the probe calibration equation. A correction was also necessary on the measured film thickness to take into account capillary rise effects (between the parallel probe wires) which could not be neglected in this study of relatively low Re_L. Using the water data at $x = 8$ cm from the entry as a reference (where the film was practically smooth and its thickness known from the *Nusselt* expression), and considering the effect of surface tension on meniscus formation, a constant correction was determined for each fluid employed here.

It will be pointed out that the aforementioned spacing of the probes along the plate was selected in order to capture all possible regions of the *developing* film, as discussed in subsequent sections. Of particular interest here is the region of incipient wave formation, which is preceded by an entrance length, L_e, of smooth film. On the basis of previous experiments (e.g. Pierson and Whitaker, 1977) the length at which waves are first visible was estimated to be in the range 5 to 10 cm for water with a tendency to increase with Re_L, in the Re_L range of the present measurements. Another region of interest (the last one in sequence) is that of three-dimensional waves which, again for water, was roughly estimated (e.g. Chang, 1994) to be within 40 cm from the liquid entry point. Thus, the five probes, located between 8 and 36 cm from liquid entry, were considered sufficient to investigate film development with the three fluids employed here.

The statistical quantities and other parameters of the film thickness time records (e.g. RMS and spectra of the fluctuations, mean wave height, wavelength, wave celerity) were calculated from 10,000-point samples, obtained over a period of 80 s with a 125 Hz sampling frequency. Data sets are identified by letters (W, B1 or B2), and a number in parenthesis, designating liquid type and probe location, respectively; e.g. W_(19), B1_(19) and B2_(19) designate water, 1.5% and 2.5% butanol solutions, respectively, at a distance 19 cm from entry.

3. Visual observations

Visual studies of the flow pattern were made using a high-speed camera (*Red lake Motion Scope PCI*®). Recordings were made for all liquids examined by aligning the camera normal to one of the channel main parallel plates (Fig. 1), at various locations along the plate in order to investigate the evolution of waves on the falling film. A photoflood was also used with a diffuser just in front of the light source, to improve lighting of the main channel aiming at enhancing the images of waves. It is rather difficult to describe the flow development along the channel using only a few still pictures, instead of the original video recordings, and to clearly discern differences between liquids with different values of surface tension. Nevertheless, using some typical images, an attempt is made to describe wave evolution on the falling film for two of the liquids employed in this work; i.e. water and 2.5% butanol solution.

In Fig. 2 a general view is provided of the wave structure for water, observed in the section between 10 and 25 cm from liquid entry, for two different values of Re_L; i.e. 128 and 282. A

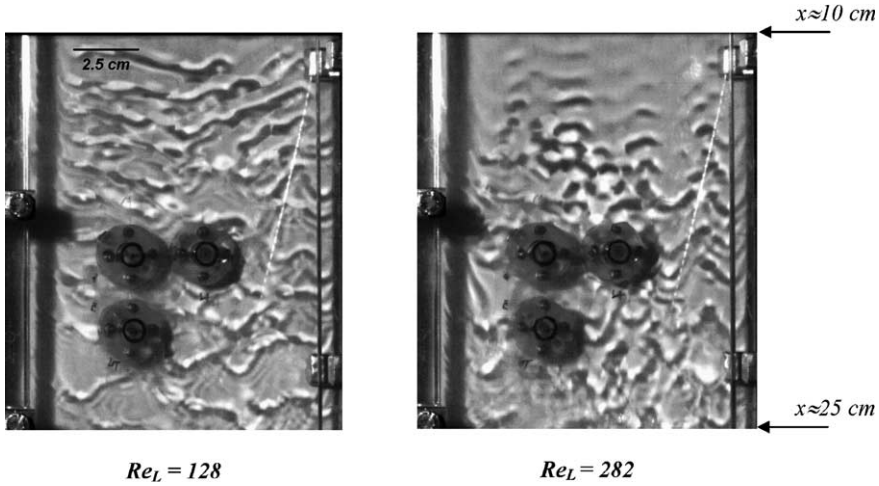

Fig. 2. A view of *water* film flow on the vertical plate for two Re_L. Distance from liquid entry is also marked in the pictures (embedded probes shown in the background).

comparatively larger wave-free area is observed at $Re_L = 282$, while at $Re_L = 128$ short waves (having small wavelength) become visible at a distance of approximately 9–10 cm from the entry of the film being nearly two-dimensional, before developing into larger 3-D waves. These wave patterns are clearly shown in Fig. 3 as well, in which both the entrance and the wave inception region just below liquid entry are depicted, with the film appearing to be initially smooth and mostly undisturbed for both cases of Re_L. Comparing the flow pattern at the wave inception region for the higher values of Re_L with that corresponding to lower Re_L, non-linear effects in the former case apparently become important at a small distance after waves appear ($\sim$1–2 wavelengths). Thus, the transition from 2-D growing perturbations to 3-D waves appears to be more abrupt at higher Re_L. Indeed, as Figs. 2 and 3 show, the initial short waves not only have steeper wave fronts, with increasing liquid flow rate, but they also evolve rapidly to larger ones with a U or W-shape. Similar trends have also been reported elsewhere (e.g. Pierson and Whitaker, 1977; Chang, 1994). Despite the aforementioned difference observed in the flow development near wave inception, waves generated in this region either at low or higher Re seem to travel downstream in a stationary manner for a relatively long distance ($\sim$10 wavelengths). Further downstream, gravity aids wave growth and long waves in the form of large tear-drop humps appear for both water and butanol solution, with short forerunner waves right in front of them covering part of the substrate film area between the larger waves, as subsequently shown. From the pictures, apart from a qualitative description of the wave evolution, one may also obtain a rough estimate of the wavelength, the value of which appears to depend both on Re_L and downstream distance. For instance, for water at the inception region (Fig. 2, $Re_L = 128$) the wavelength seems to be approximately 1 cm.

The flow development for the lower surface tension butanol solution is similar in general to that of water, as the first visible short waves are amplified downstream leading to larger solitary-type waves characterized by large humps that contain the largest portion of moving liquid mass. However, upon closer examination wave evolution appears to be somewhat different compared to

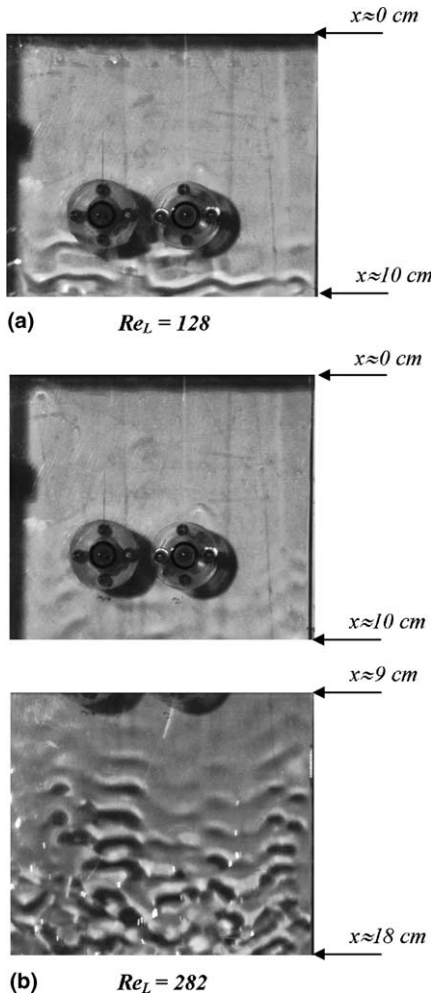

Fig. 3. The entrance and wave inception region for *water* at two Re_L: (a) 128 and (b) 282. Distance from liquid entry is also marked.

the water case, as can be seen in the pictures of Fig. 4 where views are included of the inception region for 2.5 % butanol solution at two different values of Re_L. It is evident that the waves make their appearance at a shorter distance, of approximately 5 cm from liquid entry at $Re_L = 121$, growing steeper in the downstream direction and having a less pronounced 2-D character. The same trend is observed at higher Re_L values; i.e. for the higher interfacial tension water there is a longer smooth-film entry region, compared to the butanol solution, before the first wave is observed. Another characteristic feature of the lower surface tension butanol solution are the relatively larger waves evolving on the liquid film, also evident in Fig. 5 where the wave pattern is shown at $Re_L > 200$ in a region far from the liquid entry. It may be noted that the waves (humps) for water are separated by a rather undisturbed flat film, whereas for butanol solution the film substrate in-between humps, is more disturbed as a result of the more frequent interaction

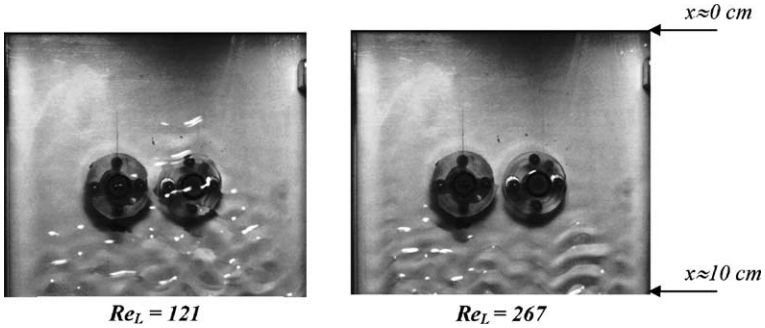

Fig. 4. The entrance and wave inception region for the *2.5% butanol solution* for two typical Re_L. Distance from liquid entry is also marked.

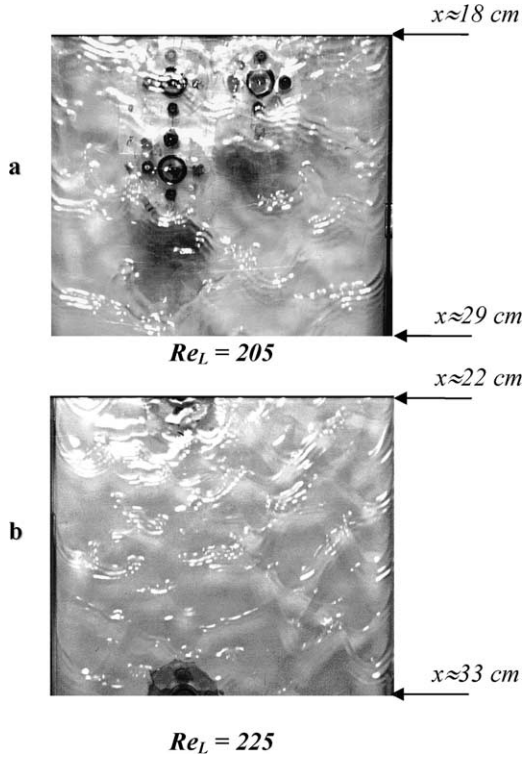

Fig. 5. Liquid film flow in the region near the end of the channel for intermediate Re_L: (a) *water* ($Ka = 3500$) and (b) *2.5% butanol solution* ($Ka = 1650$). Distance from liquid entry is also marked.

between waves. This trend is better identified in video recordings of the film of butanol solution, which appears to be almost totally covered with waves having practically no undisturbed regions. The previously referred to *forerunner waves* are clearly visible in both pictures in Fig. 5.

4. Interpretation of instantaneous film thickness data

4.1. Film thickness characteristics

The well-known *Nusselt* expressions for laminar film flow, used here as a reference, are as follows:

$$h_{\mathrm{N}} = \left(\frac{3\Gamma\mu}{\rho^2 g}\right)^{1/3} = \left(\frac{3}{4}\frac{\mu^2}{\rho^2 g}\right)^{1/3} Re_{\mathrm{L}}^{1/3} \tag{3}$$

$$u_{\mathrm{s}} = \frac{g h_{\mathrm{N}}^2 \rho}{2\mu} \tag{4}$$

$$\langle u \rangle = \frac{g h_{\mathrm{N}}^2 \rho}{3\mu} \tag{5}$$

where h_{N} is the mean film thickness, u_{s} the maximum velocity of the film at the surface and $\langle u \rangle$ the mean film velocity; Γ is the liquid mass flow rate per unit width of plate and ρ and μ are the liquid density and viscosity.

Film thickness measurements for water were made at five different stations along the middle of the plate, covering a Re_{L} range from ~60 to ~360. In Fig. 6 the experimental mean film thickness, h_{mean}, for water is presented for all measurement stations, exhibiting an increase with increasing Re_{L}, with the lower values of thickness corresponding to $x = 8$ cm (near the liquid entry), where the film is nearly flat and undisturbed. The film seems to be thicker at $x = 19$ and 22 cm compared to $x = 33$ and 36 cm especially for $Re_{\mathrm{L}} > 200$; this might be attributed to the formation of the waves near the center region of the test plate for these Re_{L}, as is also reported in a similar study by Salazar and Marschall (1978). The mean thickness at $x = 8$ cm for the three liquids tested is displayed in Fig. 7, showing a trend similar to the *Nusselt* prediction, h_{N}, as expected. Finally, in Fig. 8 average film thickness data are plotted, which are obtained with all three liquids at various locations along the plate. No clear trend is identified in these data, related to fluid properties; thus, no particular significance can be attached to differences observed between various cases.

The root-mean-square (RMS) values of film fluctuations provide a measure of "dispersion" of data about their mean value. Fig. 9 shows the dependence of RMS values, h_{RMS}, on Re_{L} at various locations for all liquids examined. Throughout the Re_{L} range, h_{RMS} is considerably smaller in magnitude compared to the mean thickness, with a tendency to increase displaying a strong dependence on Re_{L} below $Re_{\mathrm{L}} \sim 200$. Above this limit there is a noticeable reduction of such dependence and h_{RMS} values seem to remain almost constant. An interesting observation concerns data taken at $x = 8$ cm (near liquid entry), where an increase of RMS values with increasing Re_{L} is evident as already mentioned; however this increase is followed at higher Re_{L} by a very pronounced reduction of h_{RMS} towards very low values because of the displacement of wave inception region downstream. RMS values for the low surface tension butanol solutions are clearly larger compared to those for water. This tendency is expected in view of the observed (Section 3) longer wave-free entrance region corresponding to water and the nearly flat film surface at this location ($x = 8$ cm). A similar trend is observed at $x = 19$ cm, where RMS values for water seem to be lower compared to those for butanol solutions, except for the range above $Re_{\mathrm{L}} \sim 200$ in which all

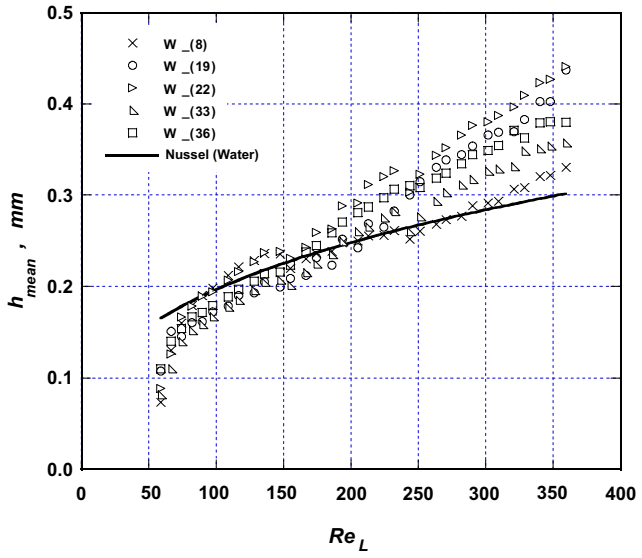

Fig. 6. Mean film thickness, h_{mean}, vs. Re_{L} for water at various locations along the test plate. Symbols are identified by liquid type and distance (in cm) from liquid entry.

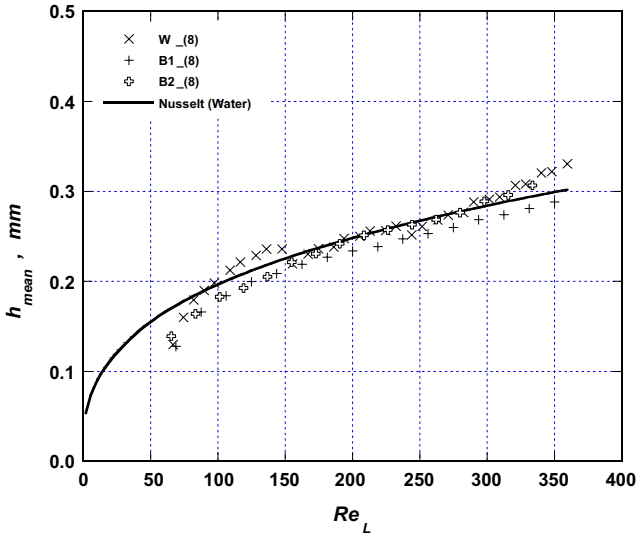

Fig. 7. Mean film thickness, h_{mean}, vs. Re_{L} for the three liquids examined, at a distance 8 cm from liquid entry, where the film is rather undisturbed.

values are comparable. On the contrary, the trend encountered at $x = 36$ cm, i.e. h_{RMS} values for water somewhat larger compared to those for butanol solutions (even though waves for the latter appear earlier), is more difficult to explain. Although experimental inaccuracies could play a role,

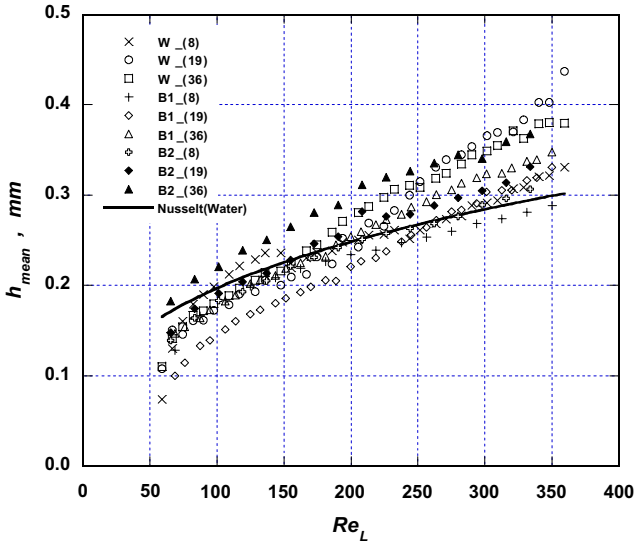

Fig. 8. Mean film thickness, h_{mean}, vs. Re_{L} for the three liquids examined at various locations along the test plate.

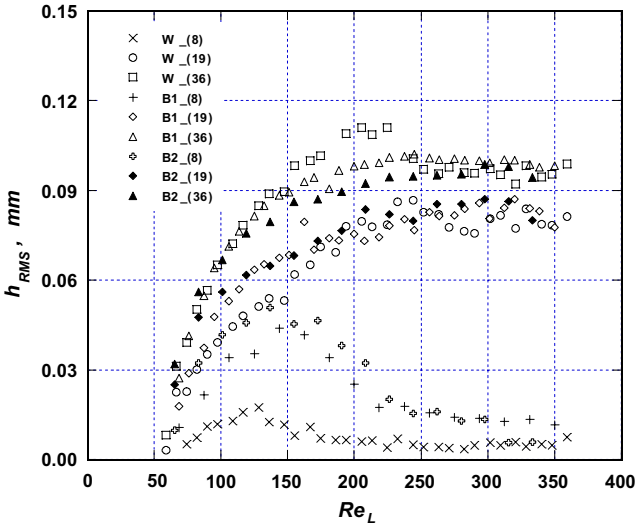

Fig. 9. RMS values of film thickness, h_{RMS}, vs. Re_{L} for the three liquids examined at various locations along the test plate.

one may offer a plausible qualitative explanation for this trend. Visual observations of the flow development (Fig. 5) show that the wave pattern for water near the end of the plate consists mainly of large humps with small forerunner waves and a fairly flat, nearly undisturbed region

separating them. On the contrary, the wave pattern for butanol solutions is different as the surface of the film seems to be more disturbed, covered to a larger extent by short waves, which seem to be present in-between large humps, leading to a more "uniformly" perturbed surface and possibly lower values for h_{RMS}.

4.2. Power spectral density

Wave frequency is an essential parameter characterizing wave type. Typical *power spectral density* (PSD) of the film thickness fluctuations at various Re_L are presented in Fig. 10 for all measurement stations and liquids examined. The power spectral density (PSD) of the film thickness has been obtained by averaging modified periodograms, as reported by Paras and Karabelas (1991). The resulting standard error on the final estimate is 8%. Fig. 10a shows spectra corresponding to a location ($x = 8$ cm) near the wave inception line. The narrow spectra for the two butanol solutions seem to be typical of an almost monochromatic growing disturbance, despite the fact that the system studied is naturally excited. This is in agreement with previous observations (e.g. Chang, 1994) of growing 2-D waves. For the higher surface tension water, the wave inception line is apparently at or below $x = 8$ cm as indicated by the very short primary peak (Fig. 10a). This is indeed confirmed by the video recordings (seen also in Fig. 3a).

Fig. 10b includes spectra at $x = 19$ cm corresponding to a region where the 2-D character of the waves is not completely lost, but three-dimensional waves seem to dominate, in the form of tear-drop humps that tend to vary in the *transverse* direction and interact with their neighbors. This wave pattern is associated with a rather broad spectrum as clearly shown in Fig. 10b. The dominant wave frequency in this region (somewhat below 20 Hz) is smaller than that of the initial 2-D waves. The modal frequency in this section appears to be weakly dependent on Re_L (slightly increasing with Re_L) with somewhat smaller values corresponding to butanol solutions. Furthermore the modal frequency tends to become more pronounced for all liquids with increasing Re_L, as the energy conveyed by the waves-related to the peak value of the spectrum-increases. Nevertheless this energy is of roughly the same magnitude for all liquids examined. Further downstream, at $x = 36$ cm (Fig. 10c), a reduced modal frequency is observed with a value close to 10 Hz as also reported elsewhere (e.g. Ambrosini et al., 2002); additionally, waves for all liquids possess the common feature of a larger amount of energy conveyed. A secondary frequency of approximately 5 Hz-also noticed by Patnaik and Perez-Blanco (1996)-seems to emerge far from liquid entry (Fig. 10c) at the higher Re_L examined and may be attributed to a "distribution" of wave energy to smaller waves, possibly the forerunner waves clearly shown in the pictures (Fig. 5). It is interesting to note that Karapantsios et al. (1989), for films falling inside a tube, determined a modal frequency of ~5Hz for $Re_L = 509$ at a very long distance ($x \approx 250$ cm) from liquid entry; compared to the present data, this may indicate a further spatial evolution of the film structure (i.e. shifting and energy re-distribution to lower frequencies) far beyond the present plate section.

4.3. Wave celerity

Celerity, c, of the surface waves is calculated by cross-correlating two film thickness signals recorded simultaneously at two neighboring locations; results for all liquids at $x \approx 19$ and 36 cm are presented in Fig. 11. Waves travel with a celerity that increases with increasing Re_L as expected

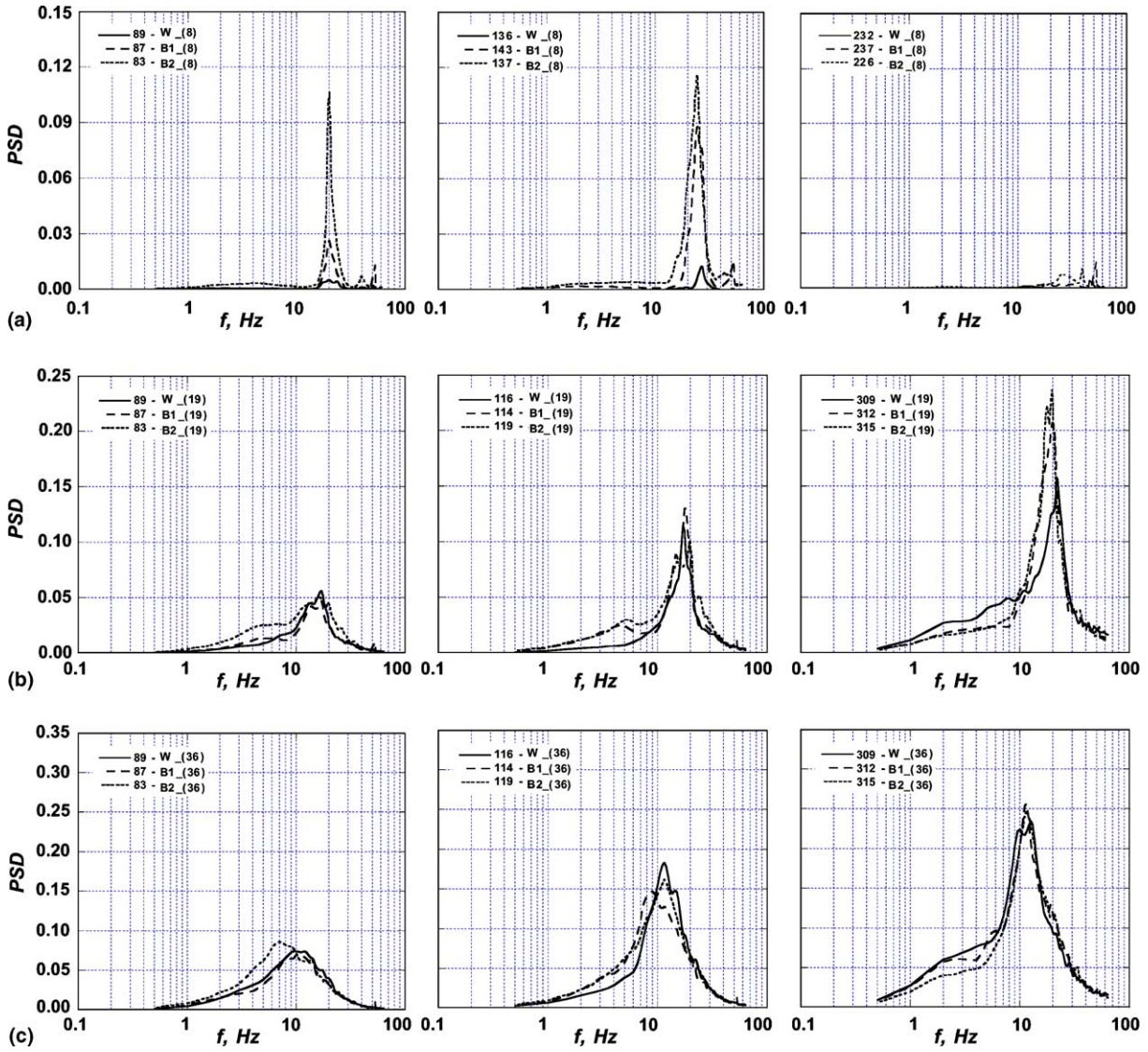

Fig. 10. Power spectra of film thickness for the three liquids examined and various Re_L, at various locations along the test plate: i.e. (a) $x = 8$ cm, (b) $x = 19$ cm and (c) $x = 36$ cm.

and also reported by various researchers in the literature (e.g. Jones and Whitaker, 1966; Ambrosini et al., 2002). This increase is pronounced in the Re_L range below ~200, in contrast with the rather modest increase of celerity at higher Re_L which is probably due to the traveling nearly stationary waves, with small alteration of their characteristics. A celerity increase with distance from the liquid entry is also evident for all liquids and may be attributed to wave interaction and to the development of larger waves that travel faster downstream. A further effort to relate the measured wave celerity with the physical properties of liquids employed is presented in a subsequent section where wave evolution is considered from the viewpoint of hydrodynamic stability.

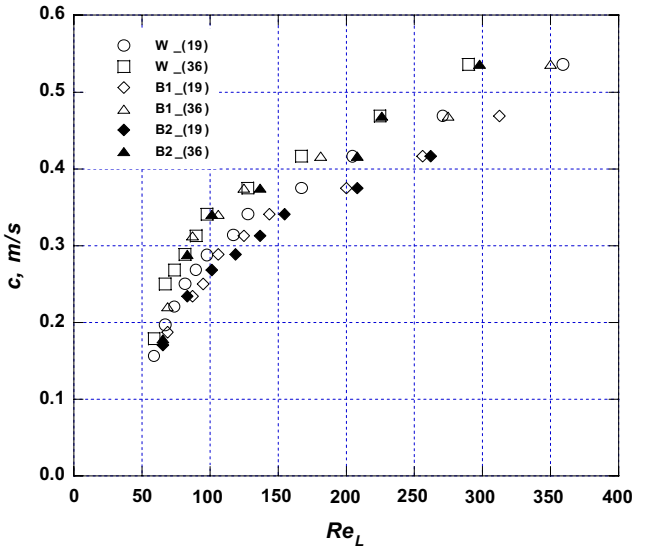

Fig. 11. Wave celerity, c, vs. Re_L for three liquids at two locations along the test plate: $x = 19$ cm and $x = 36$ cm.

It will be added that, as shown in Fig. 11, wave celerity attains somewhat larger values for the higher *Ka* number water.

4.4. Wave amplitude

A modified procedure originally proposed by Schadel (1988), as reported by Paras and Karabelas (1991), was used to determine the large wave mean amplitude, Δh_{mean}. This quantity is the mean value of the difference between a minimum in the film trace and the preceding maximum, corresponding to a large wave, for all large waves detected in a film thickness record. The dominant frequency obtained from the spectra was used as a criterion for selecting the large waves. In Fig. 12 mean wave amplitude, Δh_{mean}, for two liquids is plotted versus the corresponding Re_L at positions $x = 19$ and 36 cm. Three regions may be identified, marked A, B, C, exhibiting rather similar trends for the two liquids. These trends may be described by keeping in mind the visual observations and by taking into account the review by Chang (1994), who classified wave evolution-depending on wave type-into four regions (i.e. I–IV) within the Re_L range of the present experiments.

- *Region A*. This is a region of very strong dependence of wave amplitude on Re_L, where the values of Δh_{mean} at $x = 19$ cm seem to be larger compared to those at $x = 36$ cm. This trend may be attributed to the fact that at $x = 19$ cm strong non-linear effects dominate leading to solitary humps; the wave pattern at $x = 19$ cm possibly corresponds to Chang's region III, where waves are still growing in amplitude. On the contrary, the observed pattern at $x = 36$ cm may correspond entirely to Chang's region IV where transverse variations develop on the solitary wave crests. In this case the wave front tends to grow in the lateral direction, leading to some interaction of adjacent crests and possibly to a somewhat reduced wave amplitude.

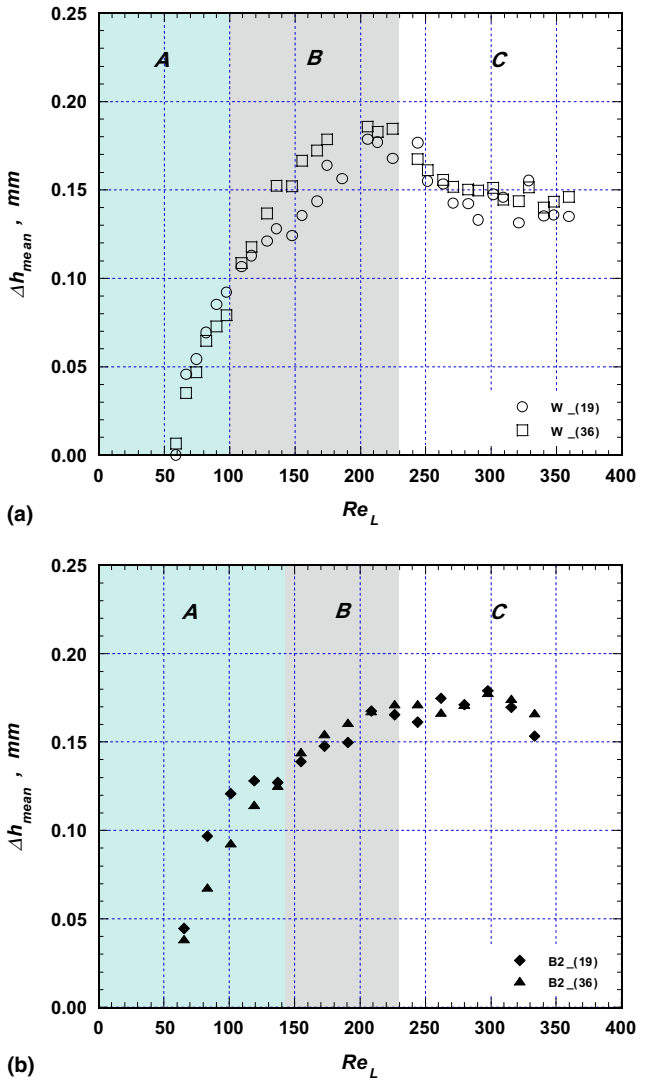

Fig. 12. Mean wave amplitude, Δh_{mean}, vs. Re_{L} at two locations ($x = 19$ and 36 cm) along the test plate for (a) water and (b) 2.5% butanol solution.

- *Region B*. At moderate Re_{L} the previous trend is reversed and waves at the bottom of the plate (at $x = 36$ cm) seem to have larger amplitude compared to that of upstream waves, as one might have expected. This difference can be attributed to the larger wavelength of the waves corresponding to this Re_{L} region, that lead to an extended length of all regimes discussed by Chang. Thus, waves at both measuring stations may correspond to Chang's region III within which waves are growing in wavelength, amplitude and speed. It is noted that there is no obvious explanation for the very pronounced peak in the amplitude variation, for the case of water (Fig. 12a) observed in this region. It is only added in support of this trend that measurements

(not presented here) corresponding to the immediately following region C show a rather thick film substrate, leading to a reduced amplitude Δh_{mean} compared to region B.

- *Region C*. For Re_{L} above ~200, waves display a tendency of reaching nearly constant amplitude independent of liquid flow rate. Considering also Figs. 9 and 11 in which a similar trend was observed for RMS values as well as in measured celerities at $Re_{\text{L}} > 250$, it may be argued that this region corresponds to traveling stationary waves that appear to dominate the film surface structure extending farther downstream, near the bottom of the channel, even if they are not two-dimensional.

It is interesting to compare the present data relatively far from liquid entry (at $x = 36$ cm) at Re_{L} high enough that amplitude growth has been drastically reduced, i.e. in region C (Fig. 12), with similar literature measurements or correlations. For this comparison, another type of estimate of wave amplitude, $\Delta h_{\max}$, is employed using the quantities $h(95\%)$ and $h(5\%)$ corresponding to thickness with probability of occurrence 95% and 5%, respectively. In Fig. 13 a generalized plot of dimensionless amplitude $\Delta h_{\max}/h_{\text{mean}}$ is shown, depicting the trend of data for vertical film flow and various liquids with fairly well-developed waves. It is pointed out that the literature data compared with data from this study correspond to the maximum value of wave amplitude estimated as the difference between the extreme minimum and maximum of the film trace. Line *I* represents a generalized empirical correlation curve presented by Alekseenko et al. (1994), which includes the dimensionless group $Re_{\text{L}}/Ka^{3/11}$ in order to take into account liquid physical properties; the Kapitza number is used here instead of a Film number, $Fi = \frac{\sigma^3}{\rho^3 g \nu^4}$, proposed by Alekseenko et al. (1994). Line *I* seems to provide a reasonable correlation for the wave amplitude

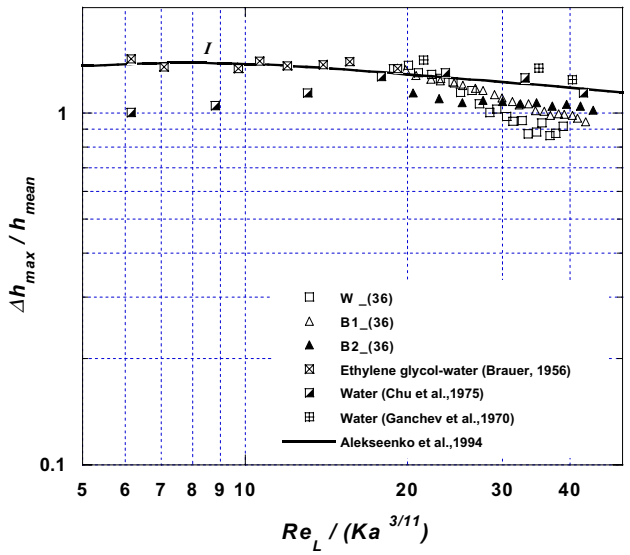

Fig. 13. Dimensionless wave amplitude $\Delta h_{\max}/h_{\text{mean}}$ vs. $Re_{\text{L}}/Ka^{3/11}$ at two locations along the test plate and comparison with literature data and empirical equation proposed.

even if flow characteristics for the liquids examined are not fully developed. Furthermore, it will be noted that the ratio $\Delta h_{max}/h_{mean}$ is near unity in this section, i.e. past the rapid wave evolution.

4.5. Wave number

In Fig. 14 an attempt is presented to relate the characteristics of developing waves with the liquid physical properties by using the dimensionless wave number k and Re_L, Ka. Here k is defined as $2\pi h_N/\lambda$, where $\lambda = c/f$ is the wavelength, with c the wave celerity and f the corresponding frequency. The data are plotted in terms of the dimensionless groups kRe_L and $Re_L/Ka^{3/11}$ as suggested by Alekseenko et al. (1994), for both *natural* and *excited (forced periodic)* two-dimensional waves. In the present work it is considered that only naturally excited waves develop, as smooth liquid entry was provided and an effort was made to isolate the experimental setup from any sources of perturbations. Line I corresponds to the initially short waves of maximum growth rate evolving near their inception region, mainly between $x = 8$ and 19 cm in the present setup. This line originates from the *two-wave equation* that describes two types of waves evolving in a vertically falling film (Alekseenko et al., 1994); i.e. those which propagate faster than the mean film velocity (and dominate in the range of large Re_L) and others that propagate slower. It is interesting that data for the three liquids are brought together quite well with the data at $x = 19$ cm being closer to line I compared to those at $x = 36$ cm. This trend may be attributed to the fact that waves at $x = 19$ cm are closer to the section of maximum growth rate whereas waves at $x = 36$ cm are three-dimensional, located farther away from that region. This implies that if measurements were made at some points near $x = 8$ cm, in the intermediate region between $x = 8$ and 19 cm, the corresponding data would probably fall close to (or along) line I.

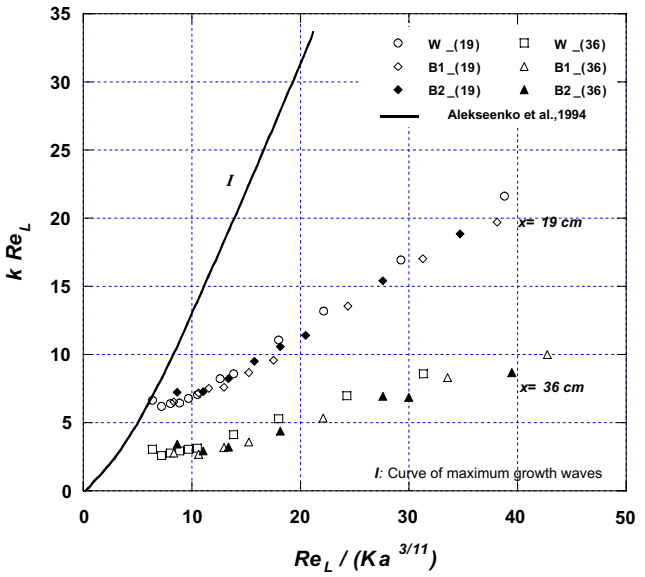

Fig. 14. Dimensionless wave number (kRe_L) vs. $Re_L/Ka^{3/11}$ at two locations along the test plate, indicating the wavy film development.

4.6. Hydrodynamic stability considerations

It is well-known that linear stability theory predicts satisfactorily the critical conditions and characteristics only of small amplitude sinusoidal waves at low Re_L. Even though analytical treatments of the Orr–Sommerfeld (OS) equation (e.g. Benjamin, 1957) have shown that the flow within a free falling film is always unstable or at least neutrally stable for all finite Re_L, a local two-dimensional model is often considered to be adequate for describing naturally occurring wave profiles, especially those evolving very close to wave inception region. For the present study, since the waves at $x = 19$ cm retain features of two-dimensionality, it is interesting to compare the respective data with theoretical results as well as with some experimental data presented in the literature. Farther downstream where wave interactions occur more frequently and lead to a chaotic spectrum of waves, wave structures display a three-dimensional pattern and linear stability theory is clearly inapplicable. Thus, in Fig. 15 data at $x = 19$ cm of dimensionless wave celerity, $C(= c/\langle u \rangle)$, are plotted versus the dimensionless group $Re_L/Ka^{3/11}$. Stability curves from linear analyses are also plotted in this figure. The relatively low values of measured celerities, C, may suggest that the waves at $x = 19$ cm are still unstable. For these values of C, periodic waves appear and continue to exist over a rather large range of celerity values, with increasing amplitude as C decreases (e.g. Nguyen and Balakotaiah, 2000). Additionally, it is noted that (considering the new data) the most unstable waves appear to be those of low-Ka 2.5% butanol solution as the corresponding dimensionless celerity C is smaller compared to that for water and 1.5% butanol solution. This is in agreement with the results of slightly non-linear analysis of OS equation using a first approximation with respect to ε ($\varepsilon = h_N/\lambda$), as Alekseenko et al. (1994) report. Comparing the present data with some experimental results from the literature, a reasonable agreement is

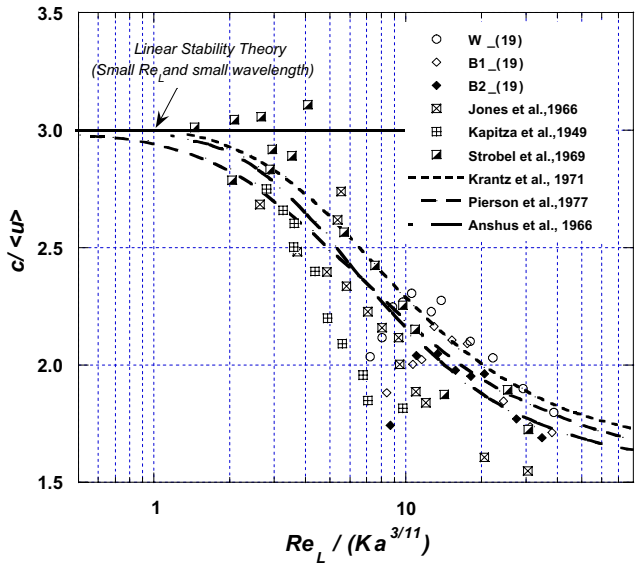

Fig. 15. Dimensionless wave celerity, $c/\langle u \rangle$, vs. $Re_L/Ka^{3/11}$ at two locations along the test plate and comparison with some literature data and stability analysis results.

observed. Furthermore, the new data are in fair agreement with numerical results for water such as those of Pierson and Whitaker (1977), who have extended the linear stability analysis to higher Re_L. Another noticeable feature in Fig. 15 is that the data from this study conform to the "equilibrium" value of C ($C_{lim} \sim 1.69$), which is the limiting velocity at large Re_L approached by solitary and periodic waves (Prokopiou et al., 1991). In Fig. 16 additional proof for the good correlation of the new celerity data is given by a comparison with the asymptotic results of the stability problem developed by Anshus (1972). It is noted that the theoretical predictions, plotted in Fig. 16, are given by the following analytical relation (also presented by Pierson and Whitaker, 1977):

$$C = 1.5(1 + 2.3428\,Ka^{2/11}\,Re_L^{-2/3}) \tag{6}$$

and correspond to an asymptotic case for large Ka and Re_L numbers.

Although linear stability theory is inadequate for describing three-dimensional waves far away from the inlet, in Figs. 17 and 18 the new data at $x = 19$ cm, are compared with some theoretical results applicable to film characteristics of large amplitude waves. A recent simplified two-dimensional model by Nguyen and Balakotaiah (2000), based on a boundary-layer (BL) analysis describes the characteristics of free falling films especially for low Re_L (2–20) and low Ka (6–22). These authors found that the following relations predict fairly accurately the maximum film thickness and wave velocity:

$$\frac{h_{max}}{h_N} - 1 = 1.925We^{-1} = 0.132Re_L^{5/3}Ka^{-1} \tag{7}$$

$$3 - C = 11.55\,We^{-1} \tag{8}$$

where $We = \frac{\sigma\langle u\rangle^2 h_N}{\rho}$ is the Weber number.

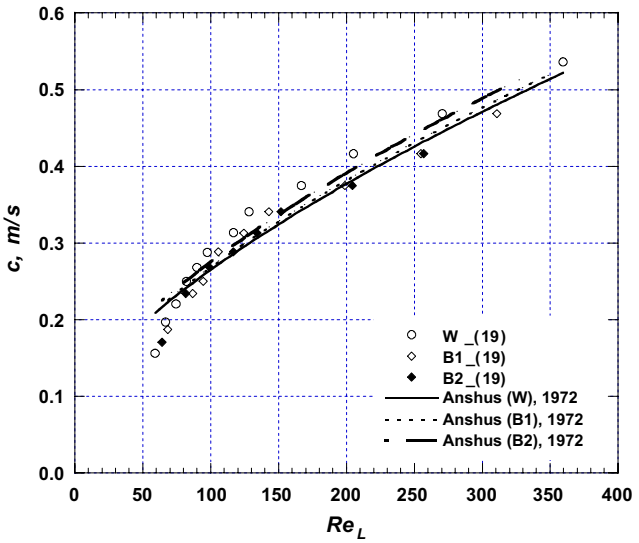

Fig. 16. Wave celerity, c, for the three liquids used at $x = 19$ cm, compared with respective predictions by Anshus (1972) based on asymptotic expression for large Re_L and Ka.

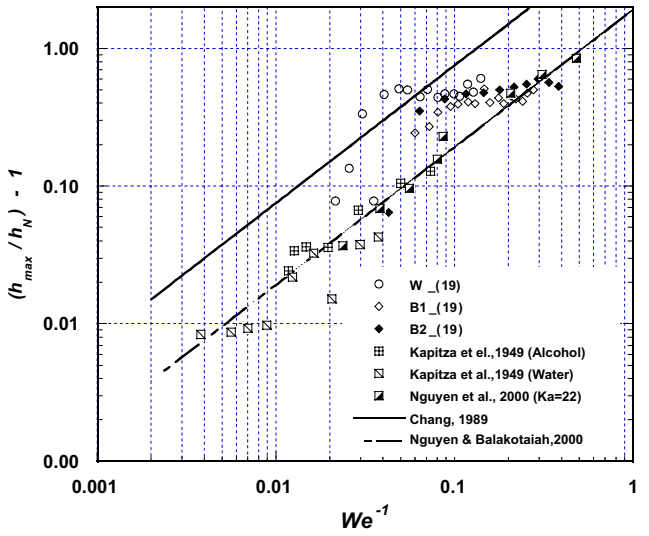

Fig. 17. Comparison of theoretical predictions of h_{max} with experimental data, using the dimensionless ratio h_{max}/h_N and *We*.

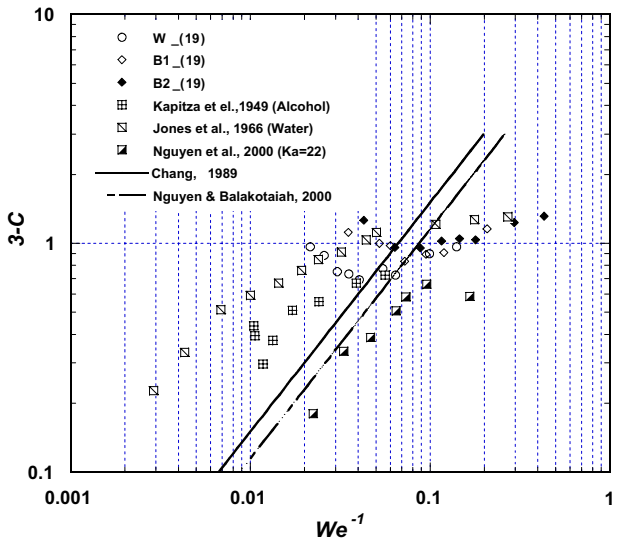

Fig. 18. Comparison of theoretical predictions on celerity with experimental data, using the dimensionless celerity 3-C and *We*.

An earlier study by Chang (1989) dealt with the analysis of steady solitary waves on a film flowing down an inclined plane near critical Re_L and was based on a non-linear treatment of long-wave (LW) approximation. The following analytical expression was obtained for the maximum wave amplitude in vertical flow:

$$\frac{h_{\max}}{h_N} - 1 = \frac{42}{25}\frac{u_s \rho g h_N^3}{v\sigma}$$

The resulting equation in dimensionless form becomes

$$\frac{h_{\max}}{h_N} - 1 = 7.56\, We^{-1} = 0.52\, Re_L^{5/3} Ka^{-1} \tag{9}$$

The dimensionless celerity of the waves is then

$$\frac{h_{\max}}{h_N} - 1 = \frac{3}{4}\left(2 - \frac{c}{u_s}\right) = \frac{1}{2}(3 - C) \quad \text{or} \quad 3 - C = 15.12\, We^{-1} \tag{10}$$

In Figs. 17 and 18 the above relations are compared with various experimental results. It is pointed out that for the new data the more representative value of h (95%) is used in place of maximum thickness, $h_{\max}$. The theoretical results in these figures have been developed for two-dimensional waves; however, the new data plotted therein are not strictly two-dimensional. Nevertheless, they tend to fall in-between the predictions of Chang (developed for low Re_L and high Ka numbers) and of Chang (1989). The latter authors report that their analysis provides physically acceptable and accurate results for low to moderate Re_L ($0 < Re_L < 100$) and a broad range of Kapitza numbers ($5 < Ka < \infty$). The celerity data for all liquids examined (Fig. 18) display more scattering than the film thickness data, as Nguyen and Balakotaiah (2000) also report, even for their own experimental data obtained with water/glycerin solutions. In their study it was also confirmed that the range of unstable wave numbers decreases as Ka (and correspondingly surface tension) increases. It appears that the new data display the same trend even though Ka for water and butanol solutions are of the same order of magnitude.

5. Concluding remarks

Visual observations suggest that the length of wave free area tends to increase with both increasing surface tension and Re_L, as expected. Concerning wave evolution far from liquid entry, no significant qualitative difference is observed between the three liquids examined, as rather large solitary-type waves in the form of tear-drop humps appear in all cases as a result of the amplification and transformation of initially short 2-D waves. However, of particular significance is the wave pattern noticed near the end of the test plate ($x \approx 30$ cm) where humps corresponding to the higher Ka water are separated by a rather undisturbed flat film, while for the lower Ka butanol solutions the film substrate on which the 3-D humps are riding, seems to be more disturbed, having no "flat" regions at all.

The increasing RMS values of film thickness fluctuations with increasing liquid rate up to $Re_L \sim 200$, are in accord with a similar increase observed (in the same Re_L range) in the mean large wave amplitude, Δh_{mean}, for all three liquids employed in this study. Additionally, for the lower Ka number butanol solutions, the appearance of waves rather close to the liquid entry is confirmed by the increased RMS values in that section.

Frequency spectra, obtained at various locations, provide a good picture of the spatial wave evolution, from the nearly monochromatic 2-D growing disturbances (relatively close to liquid

entry for low *Ka*) to the more chaotic 3-D waves downstream, represented by a broader frequency range. Furthermore, a very pronounced characteristic frequency is observed in all the spectra. This modal frequency remains nearly constant with increasing Re_L, in the range considered here, depending mainly on the distance from liquid entry. At the same time, the energy conveyed by the waves is increasing with both increasing Re_L and downstream distance having a similar magnitude up to $Re_L \sim 250$ for the three liquids employed. In the same range of higher Re_L examined here, waves of higher order corresponding to smaller frequencies seem to be amplified far downstream.

By comparing measured wave celerities with results of linear stability analyses it is confirmed that the lower *Ka* number fluids are associated with more unstable waves. Furthermore, an asymptotic expression for large Re_L and *Ka*, based on such analyses (Anshus, 1972) is in fair agreement with the celerity of developing waves.

Of particular interest, for applications involving counter-current gas–liquid flow, is the film region far from liquid entry, e.g. more than ~20 wavelengths or at distances of order 10^2 cm. This is the section where the most intensive gas/liquid interaction appears to take place in vertical counter-current flow, possibly leading to flooding (e.g. Vlachos et al., 2001). The salient features of falling film at that section, at intermediate Re_L, emerging from this work, are briefly as follows:

A 3-D wave pattern (dominated by interacting tear-drop humps) prevails, with nearly constant RMS values of film thickness fluctuations above $Re_L \sim 200$. The large wave celerity and wavelength tend to increase with Re_L and with distance; the characteristic wave frequency tends to remain unaffected by Re_L and to decrease with distance from entry. Large wave amplitude shows a dependence on Re_L similar to that of RMS; however with the exception of small Re_L this amplitude normalized with the mean film thickness, h_{mean}, appears to be nearly independent of Re_L and roughly equal to unity.

In general, the falling film characteristics obtained in this study provide new insights helpful in future modelling efforts; in particular the new data are expected to help understand the mechanism of flooding in vertical channels.

References

Adomeit, P., Renz, U., 2000. Hydrodynamics of three-dimensional waves in laminar falling films. Int. J. Multiphase Flow 26, 1183–1208.

Alekseenko, S.V., Nakoryakov, V.E., Pokusaev, B.G., 1985. Wave formation on vertical falling liquid films. Int. J. Multiphase Flow 11, 607–627.

Alekseenko, S.V., Nakoryakov, V.E., Pokusaev, B.G., 1994. Wave Flow Of Liquid Films. Beggel House, New York.

Ambrosini, W., Forgione, N., Oriolo, F., 2002. Statistical characteristics of a water film falling down a flat plate at different inclinations and temperatures. Int. J. Multiphase Flow 28, 1521–1540.

Anshus, B.E., Goren, S.L., 1966. A method of getting approximate solutions to the Orr-Sommerfeld (OS) equation for flow on a vertical wall. A.I.Ch.E. J. 2, 1004–1008.

Anshus, B.E., 1972. On the asymptotic solution to the falling film stability problem. Ind. Eng. Chem. Fund 11, 502–508.

Benjamin, T.B., 1957. Wave formation in laminar flow down an inclined plane. J. Fluid Mech. 2, 554–574.

Benney, B.J., 1966. Long waves in liquid films. J. Math. Phys. 45, 150–155.

Chang, H.-C., 1989. Onset of nonolinear waves on falling films. Phys. Fluids A 1, 1314–1327.

Chang, H.-C., 1994. Wave evolution on a falling film. Annu. Rev. Fluid Mech. 26, 103–136.

Chang, H.-C., Demekhin, E.A., Kopelevich, D.I., 1993. Nonlinear evolution of waves on a vertically falling film. J. Fluid Mech. 250, 433–480.

Chu, K.J., Dukler, A.E., 1974. Statistical characteristics of thin, wavy films: part II. Studies of the substrate and its wave structure. A.I.Ch.E. 20, 695–706.

Jones, L.O., Whitaker, S., 1966. An experimental study of falling liquid films. A.I.Ch.E. J. 12, 525–529.

Kapitza, P.L., 1964. Wave flow of thin layers of a viscous fluid. In: Collected Papers of P.L. Kapitza. Macmillan, NY.

Karapantsios, T.D., Karabelas, A.J., 1995. Longitudinal characteristics of wavy falling films. Int. J. Multiphase Flow 21, 119–127.

Karapantsios, T.D., Paras, S.V., Karabelas, A.J., 1989. Statistical characteristics of free falling films at high Reynolds numbers. Int. J. Multiphase Flow 15, 1–21.

Khesghi, H.S., Scriven, L.E., 1987. Disturbed film flow on a vertical plate. Phys. Fluids 30, 990–997.

Krantz, W.B., Goren, S.L., 1971. Stability of thin liquid films flowing down a plane. Ind. Eng. Chem. Fund. 10, 91–101.

Lin, S.P., 1974. Finite amplitude side-band stability of a viscous film. J. Fluid Mech. 63, 417–429.

Nakoryakov, V.E., Pokusaev, B.G., Radev, K.B., 1987. Waves and their effect of convective gas diffusion in falling liquid (in Russian). Zhum. Prikl. Mekh. Tekh. Fiz. 3, 95–104, cited by Alekseenko, S.V., Nakoryakov, V.E., Pokusaev, B.G., 1994. Wave Flow of Liquid Films, Beggel House, New York.

Nguyen, L.T., Balakotaiah, V., 2000. Modeling and experimental studies of wave evolution on free falling films. Phys. Fluids 12, 2236–2256.

Paras, S.V., Karabelas, A.J., 1991. Properties of the liquid layer in horizontal annular flow. Int. J. Multiphase Flow 17, 439–454.

Paras, S.V., Drosos, E.I.P., Karabelas, A.J., Chopard, F., 2001. Counter-current gas/liquid flow through Channels with corrugated walls – Visual observations of liquid distribution and flooding. Proceedings, 5th World Conference on Experimental Heat Transfer, Fluid Mechanics and Thermodynamics, Thessaloniki, September 24–28, 2001 – Celate, G.P., et al (ed's), Edizioni ETS, Pisa.

Patnaik, V., Perez-Blanco, H., 1996. Roll waves in falling films: an approximate treatment of the velocity field. Int. J. Heat Fluid Flow, 63–70.

Pierson, F.W., Whitaker, S., 1977. Some theoretical and experimental observations of the wave structure of falling liquid films. Ind. Eng. Chem. Fund. 18, 401–408.

Portalski, S., 1963. Studies of falling liquid film flow: film thickness on a smooth vertical plate. Chem. Eng. Sci. 18, 787–804.

Portalski, S., Clegg, A.J., 1972. An experimental study of wave inception on falling liquid films. Chem. Eng. Sci. 27, 1257–1265.

Prokopiou, T., Cheng, M., Chang, H.-C., 1991. Long waves on inclined films at high Reynolds number. J. Fluid Mech. 222, 665–691.

Salazar, R.P., Marschall, E., 1978. Time-average local thickness measurement in falling liquid film flow. Int. J. Multiphase Flow 4, 405–412.

Schadel, S.A., 1988. Atomization and deposition rates in vertical annular two-phase flow. Ph.D. Thesis, University of Illinois, Urbana.

Strobel, W.J., Whitaker, S., 1969. The effect of surfactants on the flow characteristics of falling liquid films. A.I.Ch.E. J. 15, 527–532.

Tailby, S.R., Portalski, S., 1962. Wave inception on a liquid film flowing down a hydrodynamically smooth plate. Chem. Eng. Sci. 17, 283–290.

Takahama, H., Kato, S., 1980. Longitudinal flow characteristics of vertically falling liquid films without concurrent gas flow. Int. J. Multiphase Flow 6, 203–215.

Trifonov, Y.Y., Tsvelodub, O.Y., 1991. Non-linear waves on the surface of a falling liquid film. Part 1. Waves of the first family and their stability. J. Fluid Mech. 229, 531–551.

Yih, C.S., 1963. Stability of liquid flow down an inclined plane. Phys. Fluids 6, 321–334.

Yu, L.-Q., Wasden, F.K., Dukler, A.E., Balakotaiah, V., 1995. Nonlinear evolution of waves on falling films at high Reynolds numbers. Phys. Fluids 7, 1886–1902.

Vlachos, N.A., Paras, S.V., Mouza, A.A., Karabelas, A.J., 2001. Visual observations of flooding in narrow rectangular channels. Int. J. Multiphase Flow 27, 1415–1430.